JOURNAL OF APPLIED POLYMER SCIENCE VOL. 21, 1421-1438 (1977)

Modified Bead-Spring Theory of Polymer Solutions. IV. Extension to Polymer Melts

A. E. EVERAGE, JR.,* and R. J. GORDON, *Department of Chemical Engineering, University of Florida, Gainesville, Florida 32611*

Synopsis

A constitutive equation which has proven quite successful in describing the nonlinear viscoelastic behavior of dilute polymer solutions is extended to the case of molten polymers. The techniques utilized are similar to those discussed by Ferry in a similar adaptation of the Rouse–Zimm Theory. The resulting model is found to quantitatively portray the shear rate dependence of the non-Newtonian viscosity and primary normal stress functions and the frequency dependence of the storage and loss moduli. Extensional flow data reported by Spearot and Metzner for two polyethylenes are well described, using parameters calculated from steady shearing measurements. Of major significance is the ability of the model to account for influences of molecular weight, molecular weight distribution, and temperature.

INTRODUCTION

One of the major goals of current rheological research is to relate viscoelastic properties of polymeric materials to measurable molecular parameters. Considerable progress toward this end has been made in the case of dilute polymer solutions through the development of idealized mechanical models of isolated macromolecules.[1-4] These models generally give reasonable predictions, however, only in the limit of small strains or deformation rates. Attempts to generalize the models have frequently led to many conceptual as well as mathematical difficulties. There has also been a large effort to modify these dilute solution theories to apply to molten polymers,[4,5] since in many ways the molten state more closely approximates the conditions assumed in the dilute solution theories.

In this work, we extend a recently developed theory of dilute polymer solutions to molten polymers by utilizing certain reasonable empiricisms adopted in similar efforts with other molecular theories, such as the Rouse–Zimm theory. The advantage of the present formulation is the success of the dilute solution theory in accurately describing a variety of *nonlinear phenomena,* such as a non-Newtonian viscosity, without additional empiricisms or modifications, in marked contrast to most other available dilute solution molecular theories (the rigid dumbbell model is a notable exception).

* Present address: Monsanto Textile Company, Technical Center, Pensacola, Florida 32575.

CONSTITUTIVE EQUATION

In a recent series of publications, we have developed an explicit constitutive equation for dilute polymer solutions which accounts for the influences of solvent power, molecular weight, and molecular weight distribution.[6–10] The constitutive equation was derived by combining an expression for the motion of the end-to-end vector of a macromolecule, as given by Ericksen's anisotropic fluid theory,[11] with the diffusion equation for the simple "dumbbell" molecular model.[3] Thus, the formulation represents a combination of continuum mechanics and molecular theory. Later developments included introduction of multiple relaxation times[10] and extension to polydisperse systems.[8,10] For the monodisperse case, our model takes the form[10]

$$\tau_j + \theta_j \frac{\overline{D}\tau_j}{Dt} = \frac{2N_A C}{M} kT\theta_j(1 - \epsilon)\mathbf{D} \tag{1}$$

$$\frac{\overline{D}\tau_j}{Dt} \equiv \frac{\partial \tau_j}{\partial t} + \mathbf{V} \cdot \nabla \tau_j - (\nabla \mathbf{V} - \epsilon \mathbf{D}) \cdot \tau_j - \tau_j \cdot (\nabla \mathbf{V}^T - \epsilon \mathbf{D}) \tag{2}$$

$$\mathbf{S} = -p\delta + 2\eta_s \mathbf{D} + \sum_{i=1}^{N} \tau_j \tag{3}$$

where $\mathbf{S}$ is the total stress, θ_j is the jth relaxation time, N_A is Avogadro's number, C is the polymer concentration, k is Boltzmann's constant, T is the temperature, $\mathbf{V}$ is the velocity, $\mathbf{D}$ is the rate of strain tensor $\frac{1}{2}(\nabla \mathbf{V} + \nabla \mathbf{V}^T)$, p is an isotropic pressure, η_s is the solvent viscosity, and ϵ is a constant which arises in Ericksen's theory[11] and is subject to the restriction

$$0 \leq \epsilon < 1.0 \tag{4}$$

In the original development of the model, the theoretical expression for θ_j was identical to the corresponding result in the Rouse–Zimm theory[1,2] and thus involved an unknown parameter h, which measured the strength of bead–bead hydrodynamic interaction. We have found, however, that the following semi-empirical relation originally proposed by Bird and Carreau,[12]

$$\theta_j = \frac{\theta_1}{\left(\frac{1+j}{2}\right)^{\alpha}} \tag{5}$$

in which α is an unknown constant and θ_1 is the primary relaxation time, yields predictions similar to those of the classical hydrodynamic interaction formulation, but in addition provides a significant reduction in computational complexity in the application of the model. From eqs. (1)–(3) and (5), we may readily obtain the following convenient expression for the primary relaxation time θ_1, in terms of the zero-shear viscosity η_0:

$$\theta_1 = \frac{(\eta_0 - \eta_s)M}{N_A C k T (1 - \epsilon) 2^{\alpha}} \cdot \frac{1}{(Z(\alpha) - 1)} \tag{6}$$

where $Z(\alpha)$ is the Riemann zeta function,[13] defined by

$$Z(\alpha) = \sum_{m=1}^{\infty} \frac{1}{m^{\alpha}}$$

The predictions of eqs. (1)–(5) are indistinguishable from those of the Rouse–Zimm theory for small-amplitude oscillatory shearing, where the latter model is known to be highly satisfactory, but provide a significant improvement in the case of steady shearing flow. For this case, our formulation yields realistic non-Newtonian viscosity and primary normal stress functions, as well as a nonzero and *negative* secondary normal stress function.[10] The Rouse–Zimm theory predicts a constant viscosity, a quadratic dependence of N_1 on shear rate, and a zero N_2. The first two of these predictions are known to hold only at vanishing small shear rates,[4] and current data on the second normal stress difference in dilute polymer solutions consistently show it to be negative and 10–50% of N_1 in magnitude.[14-18]

It is interesting to note that eqs. (1)–(3) are very similar to the well-known four-constant Spriggs model.[19] (The Spriggs time derivative has one additional isotropic term, $\frac{2}{3}(1-\epsilon)(\boldsymbol{\tau}:\mathbf{D})\boldsymbol{\delta}$; otherwise, the models are identical.) This latter constitutive equation was obtained by extending the generalized Maxwell model of linear viscoelasticity through substitution of a properly invariant time derivative. The selection of the time derivative was made on an empirical basis, since a large number of properly invariant derivatives exist. In the Spriggs formulation, the coefficient of $\mathbf{D}$ on the right-hand side of eq. (1) is treated as an unspecified constant, related to the jth relaxation time θ_j by

$$\text{coeff. of } \mathbf{D} = 2\eta_0\theta_j \Big/ \sum_{p=1}^{N} \theta_p$$

where η_0 is the zero-shear viscosity. Thus, the Spriggs model does not explicitly account for polymer concentration, molecular weight, or temperature.

EXTENSION TO MELTS

Following Ferry's adaptation of the Rouse theory to polymer melts, we introduce the following modifications to our dilute solution model: (i) η_s is eliminated in eq. (3), and (ii) C is replaced by ρ, the melt density. The primary relaxation time is then given by

$$\theta_1 = \frac{\eta_0 M}{N_A \rho k T (1-\epsilon) 2^\alpha} \cdot \frac{1}{(Z(\alpha)-1)} \tag{7}$$

Early in our analysis of experimental results on high molecular weight melts, we found that the value of θ_1 required to best fit the experimental data was usually significantly higher than that calculated on the basis of eq. (7). This suggested that the "effective molecular weight," M_E, was actually greater than the true molecular weight M. Denoting the ratio of these two quantities by K_E, eq. (7) may be written

$$\theta_1 = \frac{\eta_0 K_E M}{N_A \rho k T (1-\epsilon) 2^\alpha} \cdot \frac{1}{(Z(\alpha)-1)} \tag{8}$$

This empiricism has some precedent in the literature, being utilized in a previous study in which the Rouse–Zimm theory was compared with concentrated polymer solution data.[20,21]

To extend the model to polydisperse melts, we assume the monodisperse equations to be applicable to each molecular weight fraction, the total polymer

contribution to the stress being obtained from a summation over all fractions. In this case, the model takes the form

$$\tau_j^i + \theta_j^i \frac{\tilde{D}\tau_j^i}{Dt} = \frac{2N_A\rho kT}{M_{E,i}}(1-\epsilon)\theta_j^i \mathbf{D} \tag{9}$$

$$M_{E,i} = K_E M_i \tag{10}$$

$$\mathbf{S} = -p\delta + \sum_i \sum_j \tau_j^i \tag{11}$$

where i refers to a particular molecular weight fraction and K_E is assumed to be identical for each fraction.

The Rouse theory, extended to entangled melts, yields the result that the ith principal relaxation time is proportional to the square of the molecular weight M_i and the friction coefficient ζ:[4]

$$\theta_1^i \sim M_i^2 \zeta_E \tag{12}$$

where ζ_E is the "effective friction coefficient," the same for all molecular weights. From eqs. (9)–(12), ζ_E may be eliminated in terms of the zero shear viscosity. We find

$$\theta_1^i = \theta_w \left(\frac{M_i}{M_w}\right)^2 \tag{13}$$

where the weight-average relaxation time θ_w is given by

$$\theta_w = \frac{\eta_0 K_E M_w}{\rho RT(1-\epsilon)\, 2^\alpha [Z(\alpha) - 1]} \tag{14}$$

To describe the molecular weight distribution, the Schulz–Zimm distribution is utilized:[22,23]

$$dn = \left(\frac{z+2}{M_w}\right)^{z+1} \frac{M^z}{z!} \exp\left(\frac{-(z+2)M}{M_w}\right) dM \tag{15}$$

where dn is the fraction of macromolecules with molecular weight in the range $M, M + dM$, and z is defined by

$$\frac{z+2}{z+1} = \frac{M_w}{M_n} \tag{16}$$

Here z represents a measure of the distribution breadth and varies from -1 ($M_w/M_n = \infty$) to ∞ ($M_w/M_n = 1.0$). The complete polydisperse model is then given by eqs. (5) and (9)–(16). For a melt whose molecular weight M_w and molecular weight distribution (z) are known, the model contains four constants: α, ϵ, η_0, and K_E or θ_w. These can be readily obtained from steady or oscillatory shearing data, as illustrated below.

MODEL PREDICTIONS AND COMPARISON WITH EXPERIMENT

Steady and Oscillatory Shearing Flow

For steady shearing flow, the velocity field is of the form

$$\mathbf{V} = (Gx_2, 0, 0)$$

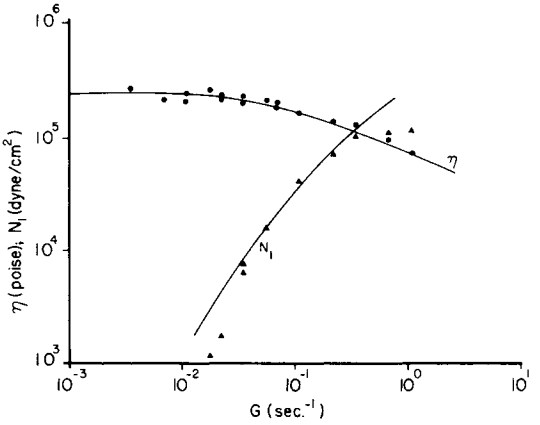

Fig. 1. Plot of η and N_1 vs. G for polyethylene melt PE-1:[25] (- - -) model prediction.

where G is the shear rate. For small-amplitude oscillatory shearing flow,

$$\mathbf{V} = (\mathrm{Re}(V_0 e^{i\omega t}),0,0)$$

Here, ω is the frequency and V_0 is a complex amplitude. For monodisperse melts, the model yields the following expressions for the non-Newtonian viscosity η, the primary and secondary normal stress differences N_1 and N_2, the dynamic viscosity η', and the dynamic storage modulus G':

$$\frac{\eta}{\eta_0} = \frac{1}{Z(\alpha) - 1} \sum_{j=2}^{N} \frac{j^\alpha}{j^{2\alpha} + (2^\alpha C\theta_1 G)^2} \tag{17}$$

$$\frac{N_1}{\eta_0} = \frac{2^{1+\alpha}\theta_1 G^2}{Z(\alpha) - 1} \sum_{j=2}^{N} \frac{1}{j^{2\alpha} + (2^\alpha C\theta_1 G)^2} \tag{18}$$

$$\frac{N_2}{\eta_0} = -\frac{2^\alpha \epsilon\theta_1 G^2}{Z(\alpha) - 1} \sum_{j=2}^{N} \frac{1}{j^{2\alpha} + (2^\alpha C\theta_1 G)^2} \tag{19}$$

$$\frac{\eta'}{\eta_0} = \frac{1}{Z(\alpha) - 1} \sum_{j=2}^{N} \frac{j^\alpha}{j^{2\alpha} + (2^\alpha \theta_1 \omega)^2} \tag{20}$$

$$\frac{G'}{\eta_0} = \frac{2^\alpha \theta_1 \omega^2}{Z(\alpha) - 1} \sum_{j=2}^{N} \frac{1}{j^{2\alpha} + (2^\alpha \theta_1 \omega)^2} \tag{21}$$

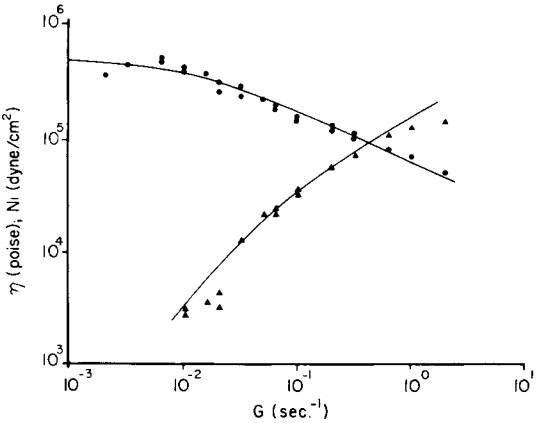

Fig. 2. Plot of η and N_1 vs. G for polyethylene melt PE-2:[25] (- - -) model prediction.

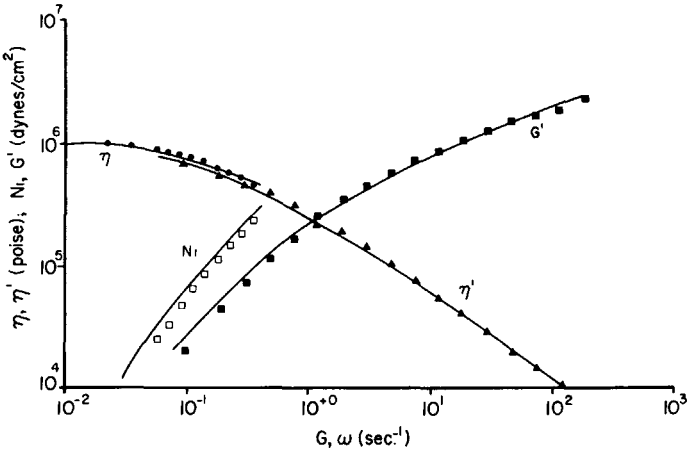

Fig. 3. Plot of η, η', and N_1 vs. G' for polyisobutylene:[26] (- - -) model prediction.

where $C^2 = \epsilon(2 - \epsilon)$. For polydisperse systems, the model predictions are

$$\frac{\eta}{\eta_0} = \frac{(z+2)^{z+3}}{(Z(\alpha)-1)\Gamma(z+3)} \int_0^\infty x^{z+2} \exp[-(z+2)x] \times \sum_{j=2}^{N} \cdot \frac{j^\alpha}{j^{2\alpha} + (2^\alpha C\theta_w G x^2)^2} dx \quad (22)$$

$$\frac{N_1}{\eta_0} = \frac{2^{1+\alpha}(z+2)^{z+2}\theta_w G^2}{(Z(\alpha)-1)\Gamma(z+2)} \int_0^\infty x^{z+4} \exp[-(z+2)x] \times \sum_{j=2}^{N} \cdot \frac{1}{j^{2\alpha} + (2^\alpha C\theta_w G x^2)^2} dx \quad (23)$$

$$\frac{N_2}{\eta_0} = \frac{-2^\alpha(z+2)^{z+2}\epsilon\theta_w G^2}{(Z(\alpha)-1)\Gamma(z+2)} \int_0^\infty x^{z+4} \exp[-(z+2)x] \times \sum_{j=2}^{N} \cdot \frac{1}{j^{2\alpha} + (2^\alpha C\theta_w G x^2)^2} dx \quad (24)$$

$$\frac{\eta'}{\eta_0} = \frac{(z+2)^{z+3}}{(Z(\alpha)-1)\Gamma(z+3)} \int_0^\infty x^{z+2} \exp[-(z+2)x] \times \sum_{j=2}^{N} \cdot \frac{j^\alpha}{j^{2\alpha} + (2^\alpha \theta_w \omega x^2)^2} dx \quad (25)$$

$$\frac{G'}{\eta_0} = \frac{2^\alpha(z+2)^{z+2}\theta_w \omega^2}{(Z(\alpha)-1)\Gamma(z+2)} \int_0^\infty x^{z+4} \exp[-(z+2)x] \times \sum_{j=2}^{N} \cdot \frac{1}{j^{2\alpha} + (2^\alpha \theta_w \omega x^2)^2} dx \quad (26)$$

where $x = M/M_w$ and $\Gamma(z)$ is the gamma function.

Equations (17)–(26) indicate the following general features of the constitutive model: (1) The second normal stress difference is predicted to be negative and

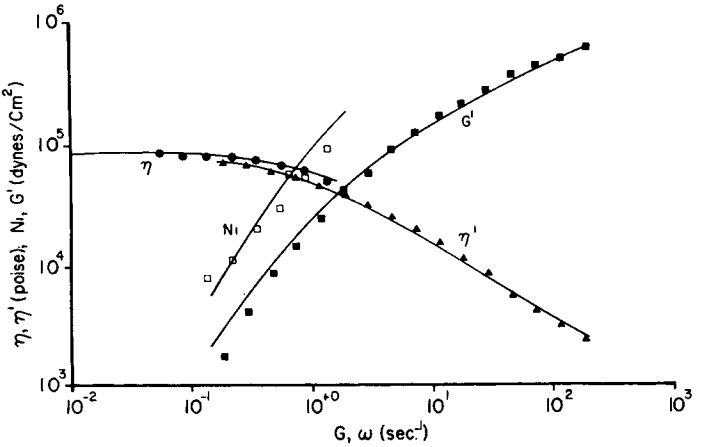

Fig. 4. Plot of η, η', N_1, vs. G' for polystyrene:[26] (- - -) model prediction.

smaller in absolute value than N_1, in agreement with recent experimental findings.[14–18] The ratio of the normal stress differences is given by

$$\frac{N_2}{N_1} = -\frac{\epsilon}{2} \tag{27}$$

(2) The following well-known analogies between material functions in steady and oscillatory shearing flow are predicted:

$$\eta(G) = \eta'(CG) \tag{28}$$

$$\frac{C^2}{2} N_1(G) = G'(CG) \tag{29}$$

Relations of this type are frequently observed experimentally.[24] (3) In the limit of high shear rates or frequencies, the model predicts a constant limiting slope for all material functions. For example, a plot of log η versus log G attains a constant slope S in the high shear rate region given by

$$S_\eta = \frac{1-\alpha}{\alpha} \tag{30}$$

The corresponding slope for log N_1 versus log G is

$$S_{N_1} = \frac{1}{\alpha} \tag{31}$$

The predictions of eqs. (14)–(23) are compared with experimental results in Figures 1–11. In these comparisons, the values of the model parameters have been determined using graphic techniques. In most cases, non-Newtonian viscosity data are available, and the parameter α is determined through eq. (30) from the experimentally observed power law slope. Assuming that z is known from measured or estimated values of M_w and M_n, a dimensionless plot of η/η_0 as a function of $C\theta_w G$ is calculated from eq. (22) and superimposed on the experimental data by suitable vertical and horizontal shifts. The value of η_0 is obtained from the vertical displacement of the dimensionless plot, and the product $C\theta_w$ is obtained from the horizontal shift. Thus, the parameters α and

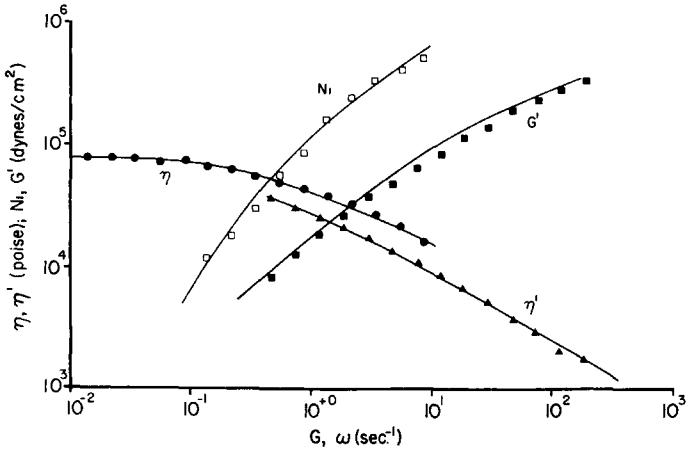

Fig. 5. Plot of η, η', N_1, vs. G' for polyethylene:[26] (- - -) model prediction.

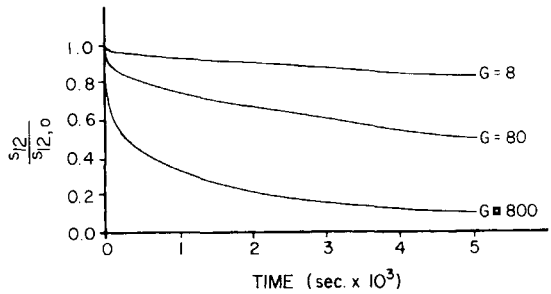

Fig. 6. Shear stress relaxation following cessation of steady shearing flow.

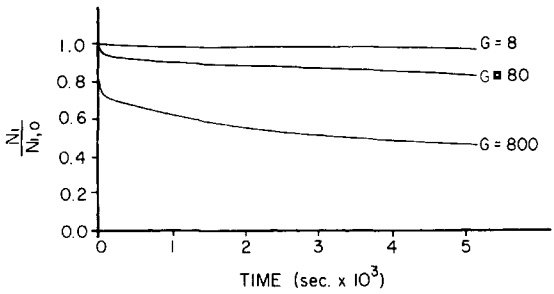

Fig. 7. Normal stress relaxation following cessation of steady shearing flow.

η_0 and the product $C\theta_w$ are obtained from viscosity data (over a suitably wide range of shear rate).

In general, data for any other material function may be used to determine the separate values of C ($= [\epsilon(2 - \epsilon)]^{1/2}$) and θ_w. If η' data are available, the value of C may be determined, as suggested by eq. (28), from the horizontal shift required to superimpose the η and η' data. Also, if experimental results for N_1 are available, a dimensionless plot of $C^2\theta_w N_1/\eta_0$ as a function of $C\theta_w G$, calculated from eq. (23), may be superimposed on the experimental data to determine the

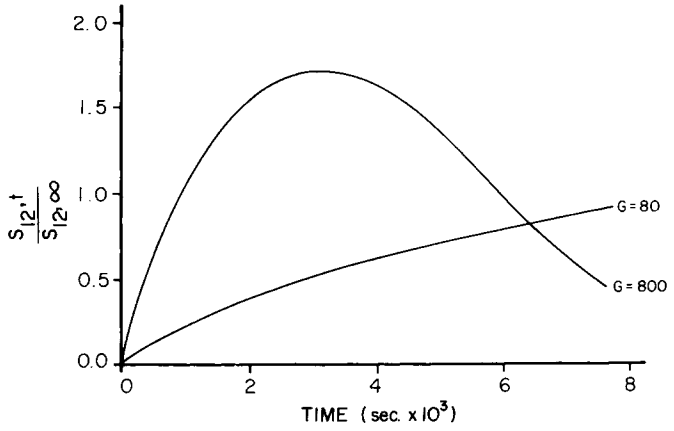

Fig. 8. Shear stress growth at inception of steady shearing flow.

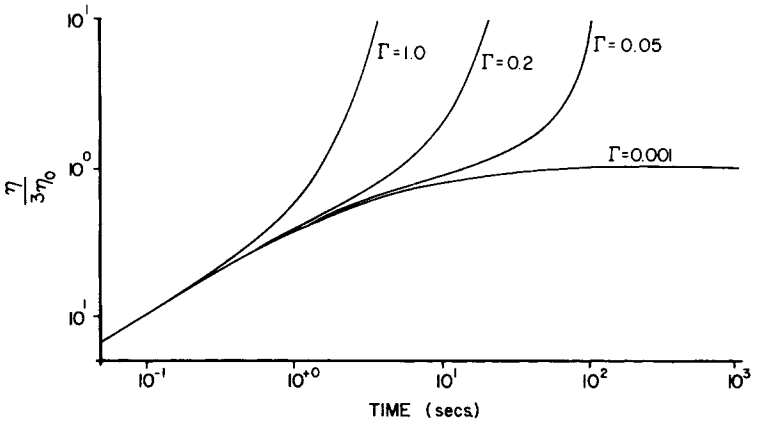

Fig. 9. Plot of $\bar{\eta}/3\eta_0$ vs. time for various extension rates.

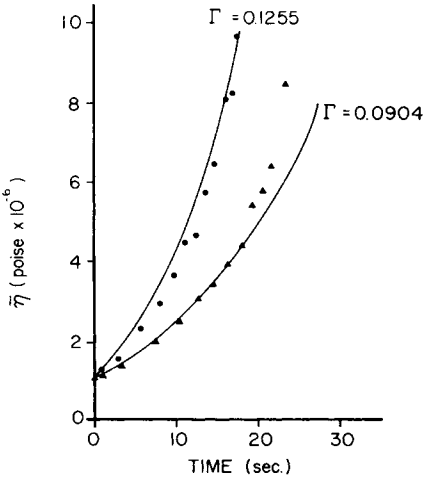

Fig. 10. Plot of $\bar{\eta}$ vs. time for polyethylene PE-1:[25] (- - -) model prediction.

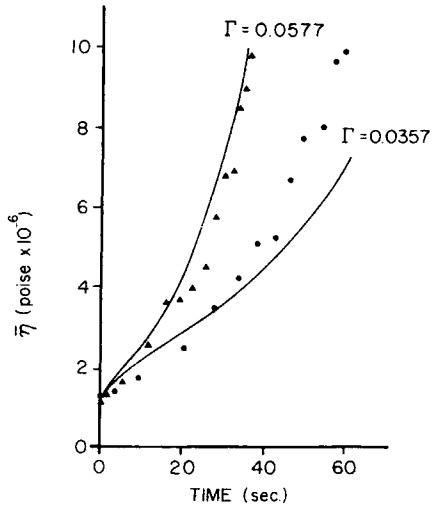

Fig. 11. Plot of $\bar{\eta}$ vs. time for polyethylene PE-2:[25] (- - -) model prediction.

quantity $C^2\theta_w/\eta_0$ from the vertical displacement of the plot. This result is then combined with the known values of η_0 and $C\theta_w$ to separately specify C and θ_w.

Spearot and Metzner[25] have recently published measurements of the non-Newtonian viscosity and primary normal stress difference for very broad molecular weight distribution polyethylene melts. Measurements of M_w, M_n, and other physical properties of these melts are tabulated in Table I, and the experimental viscosity and normal stress data are plotted in Figures 1 and 2. The predictions of eqs. (22) and (23) have been compared to these data, with the results indicated by the solid lines in the two figures. The model parameters are tabulated in Table II. The predicted results for the viscosity are quite good in both figures, being well within the experimental error. The normal stress predictions are also very good over the intermediate range of shear rates. However, discrepancies occur at low and high shear rates.

TABLE I
Physical Properties of Polyethylene Melts[25]

Polyethylene	Density, g/cc at 25°C	Melt index	$M_w \times 10^{-5}$	M_w/M_n
PE-1	0.92	1.9	3.9	11.5
PE-2	0.92	1.4	4.25	8.5

TABLE II
Model Parameters for Polyethylene Melts[25]

Polyethylene	η_o, poises $\times 10^{-5}$	ϵ	α	θ_w, sec	K_E	$\bar{\eta}$ $(t = 0)$, poises $\times 10^{-6}$
PE-1 (T = 150°C)	2.5	0.0765	2.35	9.5	6.05	1.05 (Γ = 0.1255) 1.07 (Γ = 0.0904)
PE-2 (T = 175°C)	5.0	0.274	2.35	34.3	8.34	1.23 (Γ = 0.0357) 1.17 (Γ = 0.0577)

Denson and co-workers[26] have recently published measurements of η, N_1, η', and G' for a variety of polymer melts. Their results for a low-density, branched polyethylene ($M_w = 1.8 \times 10^5$, $M_w/M_n = 6.1$), a commercial polystyrene ($M_w = 1.8 \times 10^5$, $M_w/M_n = 2.6$), and a polyisobutylene ($M_w = 5.9 \times 10^4$, $M_w/M_n = 3.0$) are plotted in Figures 3–5.

The model parameters have been determined for these data using the graphic procedures outlined above. However, for this case, the parameter α was determined from the slope of the η' data in the power law region, since this material function was measured over a very broad range of frequencies. The model predictions are represented by the solid lines in the figures, and the corresponding model parameters are tabulated in Table III. The results indicate an exceptionally good overall fit of the model to these data. In particular, it is interesting that the present theory, which is based on a linear polymer model, yields excellent results for the branched polyethylene (Fig. 5).

In summary, the present model appears to predict quite accurately the shear rate and frequency dependence of the material functions η, N_1, η', and G' for polymer melts.

Transient Stress Phenomena

For the case of a polydisperse solution in steady shearing motion which is suddenly stopped at $t = 0$, the present model yields the following expressions for the shear and normal stress relaxation for $t \geq 0$:

$$\frac{S_{12}}{S_{12,0}} = \frac{\int_0^\infty x^{z+2} \exp[-(z+2)x] \sum_{j=2}^{N} \frac{j^\alpha \exp[-tj^\alpha/2^\alpha\theta_w x^2]}{j^{2\alpha} + (2^\alpha C\theta_w G x^2)^2} dx}{\int_0^\infty x^{z+2} \exp[-(z+2)x] \sum_{j=2}^{N} \frac{j^\alpha}{j^{2\alpha} + (2^\alpha C\theta_w G x^2)^2} dx} \tag{32}$$

$$\frac{N_1}{N_{1,0}} = \frac{\int_0^\infty x^{z+4} \exp[-(z+2)x] \sum_{j=2}^{N} \frac{\exp[-tj^\alpha/2^\alpha\theta_w x^2]}{j^{2\alpha} + (2^\alpha C\theta_w G x^2)^2} dx}{\int_0^\infty x^{z+4} \exp[-(z+2)x] \sum_{j=2}^{N} \frac{1}{j^{2\alpha} + (2^\alpha C\theta_w G x^2)^2} dx} \tag{33}$$

where $S_{12,0}$ and $N_{1,0}$ are the value of S_{12} and N_1 at $t = 0$.

Equations (32) and (33) are plotted in Figures 6 and 7, for various initial shear rates. These results have been obtained assuming the typical parameter values

TABLE III
Model Parameters for Experimental Data[a] of Denson[26]

Polymer	Temperature, °C	η_0, poises	ϵ	α	θ_w, sec	K_E
Polyisobutylene	25	1.0×10^6	0.3290	3.8	3.34	1.29
Polystyrene	199	8.7×10^4	0.1310	3.2	0.761	2.54
Polyethylene	200	7.8×10^4	0.0596	2.8	1.99	7.06

[a] Melt densities were not reported; K_E values based on an assumed density of 1.0 g/cc.

$\alpha = 3$, $z = 0$, $\theta_w = 1.0$, and $\epsilon = 0.22$. The results indicate that the predicted relaxation rates increase with initial shear rate for both $S_{1,2}$ and N_1. Furthermore, the shear stress relaxes much more quickly, for a given shear rate, than the normal stress. Both of these effects are generally observed experimentally for concentrated solutions and melts.

For the case of stress growth at the inception of steady shearing flow, the melt is taken to be at rest until $t = 0$, at which time a steady shearing motion is suddenly imposed. For a polydisperase solution, the prediction of the present model for the stress growth for $t > 0$ is given in eq. (34). Here, $S_{12,t}$ and $S_{12,\infty}$ are the stress at time t and the ultimate steady-state stress, respectively.

Equation (34) is plotted in Figure 8 for the parameter values used in the stress relaxation calculation:

$$\frac{S_{12,t}}{S_{12,\infty}} = \int_0^\infty x^{z+2} \exp(-(z+2)x) \sum_{j=2}^{N} \frac{j^\alpha}{j^2 + (C_2 x^2)^2} \times \left\{1 - \exp\left(\frac{-tj^\alpha}{2^\alpha \theta_w x^2}\right)\left(\cos(CGt) - \frac{C_2 x^2}{j^\alpha}\sin(CGt)\right)\right\} dx \times \left[\int_0^\infty x^{z+2} \exp[-(z+2)x] \sum_{j=2}^{N} \frac{j^\alpha}{j^{2\alpha} + (C_2 x^2)^2} dx\right]^{-1} \tag{34}$$

where $C_2 = 2^\alpha C \theta_w G$

$$x = M/M_w, \quad C = [\epsilon(2-\epsilon)]^{1/2}$$

The results indicate that for high shear rates, stress overshoot followed by undershoot is predicted. With decreasing shear rate, however, the overshoot and undershoot ultimately disappear. Both of these effects are observed experimentally.[27–29]

The results in Figures 6–8 are in qualitative agreement with generally accepted experimental results. However, the ability of the present model to quantitatively describe transient stress phenomena is subject to question at this time. In a recent publication,[29] Chen and Bogue have reported extensive experimental measurements of time-dependent stresses in polymer melts. These authors have also compared the predictions of several constitutive equations to these experimental data. The results strongly suggest that in order to obtain quantitative agreement with experiment for transient stress phenomena, a deformation rate-dependent relaxation time is required. As noted by Graessley,[30] a deformation rate-dependent relaxation spectrum in concentrated solutions and melts may be attributed to a decrease in entanglement density with increasing shear rate (i.e., with fewer entanglement restrictions, the macromolecule may "relax" more quickly). Although the present theory accounts for friction effects from entanglement constraints in ζ_E, no attempt has been made to incorporate any effects of variations in entanglement density. Therefore, if changes in entanglement density do, in fact, affect the relaxation spectrum, further modification of the theory will be required.

EXTENSIONAL FLOW

In the previous sections, our theory was evaluated by comparing the predicted material behavior with experimental results for shearing motions. Although

these comparisons are definitely a valid measure of the accuracy of the theory, a much more rigorous test of a constitutive equation lies in its ability to predict material response under a variety of kinematic conditions. In particular, the prediction of material behavior for a given flow field (e.g., extensional flow), utilizing model parameters determined by comparisons with experiment in a distinctively different flow (e.g., shearing flow), is a uniquely severe test of the validity and internal consistency of a mechanical theory. This is especially true for extensional motion in light of the large variations in predicted stress levels and material behavior which have been reported.[31-33]

Under the restriction of constant volume, pure extensional flow is described by a velocity field of the form

$$\mathbf{V} = \Gamma(t)x_1, \qquad -\frac{1}{2}\Gamma(t)x_2, \qquad -\frac{1}{2}\Gamma(t)x_3$$

where $\Gamma(t)$ is the extension rate, which may be an arbitrary function of time. For this flow, the fluid is characterized by an extensional viscosity $\bar{\eta}$, defined by

$$\bar{\eta} = \frac{S_{11}}{\Gamma}$$

where S_{11} is the axial stress. For the case of zero force acting on the surface of the material perpendicular to the direction of extension (i.e., $S_{22} = S_{33} = 0$), $\bar{\eta}$ may be expressed in the form

$$\bar{\eta} = \frac{S_{11} - S_{22}}{\Gamma} = \frac{N_1}{\Gamma}$$

For the case of a polydisperse melt, subjected to a constant extension rate Γ and unstressed at $t = 0$, the present model yields

$$\begin{aligned}\frac{\bar{\eta}}{3\eta_0} = {} & \frac{(z+2)^{z+2}}{(Z(\alpha)-1)\Gamma(z+2)} \int_0^\infty x^{z+2} \exp[-(z+2)x] \\ & \times \sum_{j=2}^{N} \frac{j^\alpha}{(j^\alpha - 2C_1x^2)(j^\alpha + C_1x^2)} \\ & \times \left\{1 - \frac{2}{3}\left(1 + \frac{c_1x^2}{j^\alpha}\right) \exp\left(-(j^\alpha - 2c_1x^2)\frac{t}{\theta_w 2^\alpha x^2}\right)\right. \\ & \left. - \frac{1}{3}\left(1 - \frac{2c_1x^2}{j^\alpha}\right) \exp\left(-(j^\alpha + c_1x^2)\frac{t}{\theta_w 2^\alpha x^2}\right)\right\} dx \end{aligned} \tag{35}$$

where $c_1 = (1 - \epsilon)2^\alpha\theta_w\Gamma$.

Equation (35) has been plotted in Figure 9 for the parameter values $\epsilon = 0.2$, $\alpha = 4$, $z = 0$, $\theta_w = 3.125$ and the indicated values of Γ. The results indicate a limiting value of $\bar{\eta}$ for very low deformation rates and an exponential increase for larger values of Γ. These results are qualitatively identical to experimental observations reported by Meissner[34] and, more recently, by Everage and Ballman.[35]

Quantitative evaluation of our model requires measurements of extensional viscosity of materials which have also been characterized in shearing flow. Spearot and Metzner[25] have reported results of this type for three polyethylene melts. Extensional viscosities were obtained from measurements in a fiber spinning apparatus, and viscosity and primary normal stress difference mea-

surements were independently obtained in steady shearing flow. These data were used by Spearot and Metzner to evaluate the predictive ability of five constitutive theories: the Bird-Carreau model,[12] the Bogue-White model,[36] a modified (nonlinear) Maxwell model, a generalized Maxwell model (i.e., a nonlinear Maxwell model generalized to include two relaxation times), and the elastic dumbbell model,[3] which was modified by the inclusion of a factor accounting for finite extensibility in the polymer molecule. The parameters in these models were determined by comparison with the shearing data and the results used to predict the elongational viscosities observed in the fiber spinning experiments.

From a qualitative point of view, all five constitutive equations predicted major experimental trends correctly. However, only the generalized Maxwell model, which required the determination of five unknown constants, provided a semiquantitative description of both the shearing and extensional flows. In the remainder of this section, the analysis of Spearot and Metzner is repeated, using the present continuum-modified multibead/spring model.

The model predictions for η and N_1, eqs. (22) and (23), were fitted to the experimental viscosity and normal stress data for two of the polyethylene melts (designated by Spearot as PE-1 and PE-2) in the previous section. The experimental data and model predictions are plotted in Figures 10 and 11, and the model parameters are tabulated in Table II. Measurements of M_w and M_n for these melts were also reported by Spearot. These data and other physical properties are tabulated in Table I.

The fiber spinning apparatus used by Spearot and Metzner was operated isothermally. Polymer samples were extruded through a single orifice ($D = 0.1$ in., $L/D = 1.1$), and the resulting filaments were collected under tension on a take-up reel. The tension $T(x)$ in the filament was measured and corrected for a small amount of sag in the horizontal spin line. The extension rates were determined from the measured mass flow rates and the diameter attenuation rates, which were obtained from photographs of the spinline. The extension rate Γ was found to be constant along the spinline, and the extensional viscosity was calculated from

$$\bar{\eta}(x) = \frac{4T(x)}{\pi D^2(x)\Gamma}$$

where $D(x)$ is the filament diameter at position x.

The amount of time the fluid element at position $x = L$ had existed in the flow field was calculated from the relation

$$t = \int_0^L \frac{1}{v}\, dx$$

Thus, combining the calculations of $\bar{\eta}(x)$ and $t(x)$, the extensional viscosity was determined as a function of time for each extension rate. The results are plotted in Figures 10 and 11.

The theoretical prediction of the stress in the spinline requires the solution of the constitutive equation for the case of extensional flow at constant Γ for a fluid initially exhibiting stress levels S_{11}^0 and S_{22}^0. Under these conditions, the present model yields the following expression for the time dependent extensional viscosity:

$$\frac{\bar{\eta}}{3\eta_0} = \frac{S_{11}^0}{3\eta_0\Gamma}\sum_{j=2}^{N}\exp\left(-(j^\alpha - 2c_1)\frac{t}{\theta_w 2^\alpha}\right) - \frac{S_{22}^0}{3\eta_0\Gamma}\sum_{j=2}^{N}\exp\left(-(j^\alpha + c_1)\frac{t}{\theta_w 2^\alpha}\right)$$
$$+\frac{(z+2)^{z+2}}{(Z(\alpha)-1)\Gamma(z+2)}\int_0^\infty x^{z+2}\exp\left[-(z+2)x\right]\sum_{j=2}^{N}\frac{j^\alpha}{(j^\alpha - 2c_1x^2)(j^\alpha + c_1x^2)}$$
$$\times\left\{1 - \frac{2}{3}\left(1 + \frac{c_1x^2}{j^\alpha}\right)\exp\left(-(j^\alpha - 2c_1x^2)\frac{t}{\theta_w 2^\alpha x^2}\right)\right.$$
$$\left. -\frac{1}{3}\left(1 - \frac{2c_1x^2}{j^\alpha}\right)\cdot\exp\left(-(j^\alpha + c_1x^2)\frac{t}{\theta_w 2^\alpha x^2}\right)\right\}dx \quad (36)$$

where $c_1 = (1-\epsilon)2^\alpha\theta_w\Gamma$ and $x = M/M_w$.

In Spearot's analysis, the initial stress S_{22}^0 was taken as zero, since S_{22}^0 is smaller than S_{11}^0 and is multiplied by an exponential that decays in time. Also, Spearot retained only the longest relaxation time in the term multiplied by S_{11}^0 in each of the constitutive equations considered. This assumption allowed the stress S_{11}^0 to be equated to the initial (i.e., $x = 0$ or $t = 0$) tensile stress measured. These simplifications are also utilized in the present analysis, and eq. (36) thus reduces to

$$\frac{\bar{\eta}}{3\eta_0} = \frac{S_{11}^0}{3\eta_0\Gamma}\exp\left(-(2^\alpha - 2c_1)\frac{t}{\theta_w 2^\alpha}\right) + \frac{(z+2)^{z+2}}{(Z(\alpha)-1)\Gamma(z+2)}$$
$$\times\int_0^\infty x^{z+2}\cdot\exp\left[-(z+2)x\right]\sum_{j=2}^{N}\frac{j^\alpha}{(j^\alpha - 2c_1x^2)(j^\alpha + c_1x^2)}$$
$$\times\left\{1 - \frac{2}{3}\left(1 + \frac{c_1x^2}{j^\alpha}\right)\cdot\exp\left(-(j^\alpha - 2c_1x^2)\frac{t}{\theta_w 2^\alpha x^2}\right)\right.$$
$$\left. -\frac{1}{3}\left(1 - \frac{2c_1x^2}{j^\alpha}\right)\cdot\exp\left(-(j^\alpha + c_1x^2)\frac{t}{\theta_w 2^\alpha x^2}\right)\right\}dx \quad (37)$$

where $c_1 = (1-\epsilon)2^\alpha\theta_w\Gamma$ and $x = M/M_w$.

Equation (37) has been evaluated using the parameter values determined from the shearing data (Table II) and the experimentally measured values of S_{11}^0 (also tabulated in Table II in the form $\bar{\eta}(0) = S_{11}^0/\Gamma$). The predictions are represented by the solid lines in Figures 10 and 11.

The results are very encouraging. The model predictions describe quite well the higher extension rate data for both polyethylenes. For the lower extension rates, the model predictions clearly underestimate $\bar{\eta}$ at large values of t. However, it should be emphasized that this degree of discrepancy is well within the experimental scatter in the shear data from which the model parameters were determined.

In summary, the present model appears to satisfactorily describe the extensional flow field of an isothermal melt spinning experiment, using model parameters determined from steady shearing flow. Furthermore, the present theory offers a significant improvement in predictive capability, with fewer adjustable parameters than the constitutive equations evaluated by Spearot and Metzner.

INFLUENCE OF TEMPERATURE

It is highly desirable that a constitutive equation have the inherent ability to predict the influence of temperature on rheological behavior. Previous studies

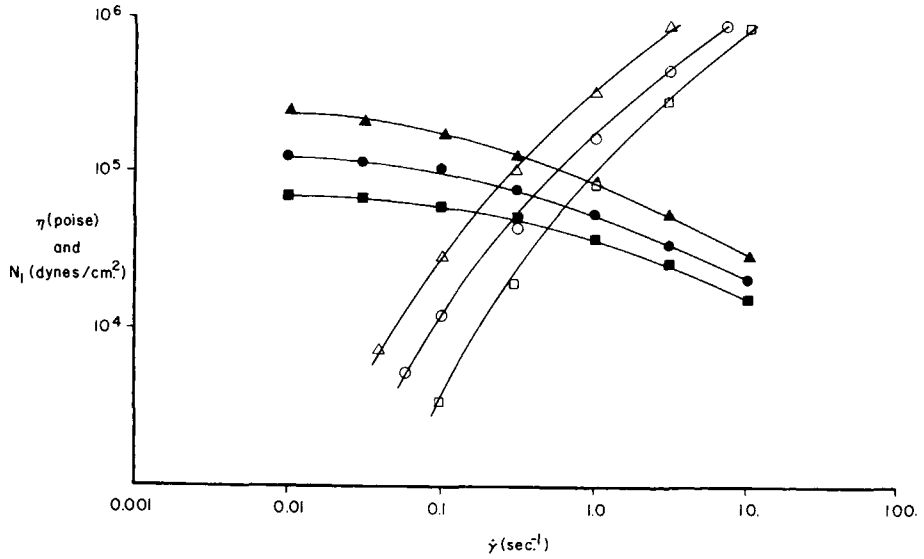

Fig. 12. Plot of η (solid points) and N_1 (open points) vs. shear rate at three temperatures: (Δ) 160°C; (○) 180°C; (□) 200°C. Data of Chen and Bogue.[29]

have indicated that the primary effect of temperature is on the polymer relaxation time, while the relative shapes of the viscosity or normal stress curves remain unchanged. The dependence of θ_w on T is given by eq. (14); and if we assume ϵ and α are independent of temperature, this expression suffices to determine completely the rheological changes.

From eqs. (14) and (22), one may readily demonstrate that curves of η/η_0 versus G at different temperatures should superimpose if G is multiplied by a "shift factor" a_T, defined by

$$a_T = \eta_0 \rho_R T_R / \eta_{0R} \rho T \tag{38}$$

where T_R, ρ_R, and η_{0R} are the reference temperature, density, and viscosity, respectively. Similarly, plots of $N_1 \rho_R T_R / \rho T$ versus $a_T G$ should also superimpose. Ferry has previously presented both of these reduced variable correlations and noted their success in correlating a variety of data.[4] Mendelson[37] has also demonstrated the success of the viscosity correlation for a wide variety of polymers, with a_T calculated from the "approximate form,"

$$a_T \approx \eta_0 / \eta_{0R}$$

An additional example of this approach is illustrated in Figures 12 and 13. In Figure 12, the viscosity and primary normal stress data of Chen and Bogue[29] is plotted for three temperatures. The data for 160° and 200°C were then shifted as discussed above. The resulting single curves in Figure 13 clearly illustrate the success of the procedure.

Under the assumed constancy of α and ϵ, the influence of temperature on any other rheological function may readily be determined.

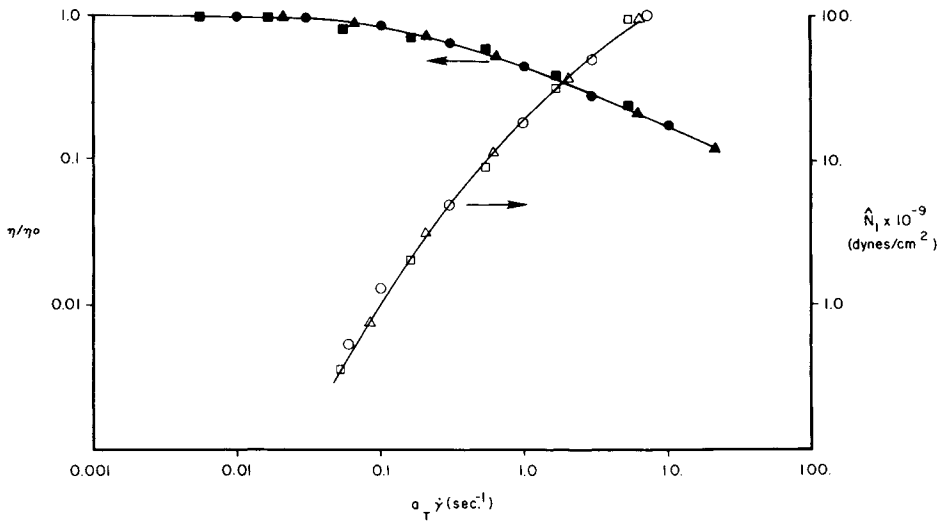

Fig. 13. Data of Fig. 12 in reduced variable form. $\hat{N}_1 = N_1 \rho_R T_R / \rho T$; $a_T = (\eta_0 \rho_R T_R)/(\eta_{OR} \rho T)$. Symbols as in Fig. 12.

SUMMARY

An explicit rheological constitutive equation for polymer melts is presented. The model contains four parameters: η_0, α, ϵ, and θ_w or K_E; it is quite similar in form to the four-constant Spriggs model. In simple shearing or small-amplitude oscillatory shearing, the model predictions yield realistic predictions of rheological response, and the model is shown to quantitatively fit a variety of experimental data. The extensional viscosity measurements of Spearot and Metzner are also well described, using parameters obtained from steady shearing. The form of the model yields well-known temperature superposition relations for viscosity and the first normal stress difference and may be used to readily predict the temperature dependence of other rheological functions.

The authors are grateful to the National Science Foundation for partial support under Grant GK 31590.

References

1. P. E. Rouse, Jr., *J. Chem. Phys.*, **21**, 1272 (1953).
2. B. H. Zimm, *J. Chem. Phys.*, **24**, 269 (1956).
3. A. Peterlin, *Pure Appl. Chem.*, **12**, 563 (1966).
4. J. D. Ferry, *Viscoelastic Properties of Polymers*, 2nd ed., Wiley, New York, 1970.
5. F. Bueche, *J. Chem. Phys.*, **20**, 1959 (1952).
6. R. J. Gordon and W. R. Schowalter, *Trans. Soc. Rheol.*, **16**, 79 (1972).
7. R. J. Gordon, and A. E. Everage, Jr., *J. Appl. Polym. Sci.*, **15**, 1903 (1971).
8. A. E. Everage, Jr., and R. J. Gordon, *J. Appl. Polym. Sci.*, **16**, 1967 (1972).
9. A. E. Everage, Jr., and R. J. Gordon, *A.I.Ch.E. J.*, **17**, 1257 (1971).
10. A. E. Everage, Jr., and R. J. Gordon, *J. Appl. Polym. Sci.*, **18**, 3137 (1974).
11. J. L. Ericksen, *Kolloid-Z.*, **173**, 117 (1960).
12. R. B. Bird, and P. J. Carreau, *Chem. Eng. Sci.*, **23**, 427 (1968); *ibid.*, **23**, 901 (1968).
13. M. Abramowitz and I. A., Stegun, *Handbook of Mathematical Functions*, Dover Publications, New York, 1965.

14. R. F. Ginn and A. B. Metzner, *Trans. Soc. Rheol.*, **13,** 429 (1969).
15. R. I. Tanner, *Trans. Soc. Rheol.*, **14,** 483 (1970).
16. M. C. Williams and O., Olabisi, *Trans. Soc. Rheol.*, **16,** 727 (1972).
17. R. I. Tanner, *Trans. Soc. Rheol.*, **17,** 365 (1973).
18. E. A. Kearsley, *Trans. Soc. Rheol.*, **17,** 617 (1973).
19. T. W. Spriggs, *Chem. Eng. Sci.*, **20,** 931 (1965).
20. J. E. Frederick, N. W. Tschoegl, and J. D. Ferry, *J. Phys. Chem.*, **68,** 1974 (1964).
21. R. B. De Mallie, Jr., H. Meyer, J. E. Birnboim, J. E. Frederick, N. W. Tschoegl, and J. D. Ferry, *J. Chem. Phys.*, **66,** 536 (1962).
22. B. H. Zimm, *J. Chem. Phys.*, **16,** 1099 (1948).
23. L. H. Peebles, Jr., *Molecular Weight Distributions in Polymers*, Interscience, New York, 1971.
24. C. D. Han, K. U. Kim, N. Siskovic, and C. R. Huang, *Rheol. Acta*, **14,** 533 (1975).
25. J. A. Spearot, and A. B. Metzner, *Trans. Soc. Rheol.*, **16,** 495 (1972).
26. C. D. Denson, W. M. Prest, Jr. and J. M. O'Reilly, *A.I.Ch.E. J.*, **15,** 809 (1969).
27. J. D. Huppler, I. F. MacDonald, E. Ashare, T. W. Spriggs, R. B. Bird, and L. A. Holmes, *Trans. Soc. Rheol.*, **11,** 181 (1967).
28. N. Nishida, D. G. Salladay, and J. L. White, *J. Appl. Polym. Sci.*, **15,** 1181 (1971).
29. I.-J. Chen, and D. C. Bogue, *Trans. Soc. Rheol.*, **16,** 59 (1972).
30. W. W. Graessley, *J. Chem. Phys.*, **47,** 1942 (1967).
31. A. S. Lodge, *Elastic Liquids*, Academic Press, New York, 1964.
32. M. J. Yamamoto, *J. Phys. Soc. Japan*, **12,** 1148 (1957).
33. R. B. Bird and T. W. Spriggs, *Phys. of Fluids*, **8,** 1390 (1965).
34. J. Meissner, *Trans. Soc. Rheol.*, **16,** 405 (1972).
35. A. E. Everage, Jr. and R. L. Ballman, *J. Appl. Polym. Sci.*, **20,** 1137 (1976).
36. D. C. Bogue, *Ind. Eng. Chem., Fundam.*, **5,** 253 (1966).
37. R. A. Mendelson, *Trans. Soc. Rheol.*, **9** (1), 53 (1965).

Received February 18, 1976